Probing α-RuCl_{3} Beyond Magnetic Order: Effects of Temperature and Magnetic Field

Stephen M. Winter, Kira Riedl, David Kaib, Radu Coldea, and Roser Valentí

Phys. Rev. Lett. **120**, 077203 — Published 15 February 2018

DOI: 10.1103/PhysRevLett.120.077203

Probing α-$RuCl_3$ Beyond Magnetic Order: Effects of Temperature and Magnetic Field

Stephen M. Winter*,[1] Kira Riedl,[1] David Kaib,[1] Radu Coldea,[2] and Roser Valentí[1]

[1] *Institut für Theoretische Physik, Goethe-Universität Frankfurt, Max-von-Laue-Strasse 1, 60438 Frankfurt am Main, Germany*

[2] *Clarendon Laboratory, University of Oxford, Parks Road, Oxford OX1 3PU, United Kingdom*

(Dated: January 16, 2018)

Recent studies have brought α-$RuCl_3$ to the forefront of experimental searches for materials realizing Kitaev spin-liquid physics. This material exhibits strongly anisotropic exchange interactions afforded by the spin-orbit coupling of the 4d Ru centers. We investigate the dynamical response at finite temperature and magnetic field for a realistic model of the magnetic interactions in α-$RuCl_3$. These regimes are thought to host unconventional paramagnetic states that emerge from the suppression of magnetic order. Using exact diagonalization calculations of the quantum model complemented by semi-classical analysis, we find a very rich evolution of the spin dynamics as the applied field suppresses the zigzag order and stabilizes a quantum paramagnetic state that is adiabatically connected to the fully polarized state at high fields. At finite temperature, we observe large redistributions of spectral weight that can be attributed to the anisotropic frustration of the model. These results are compared to recent experiments, and provide a roadmap for further studies of these regimes.

Introduction – The honeycomb magnet α-$RuCl_3$ has recently received significant attention, in view of the ongoing search for exotic magnetic states in real systems [1–8]. This material has anisotropic and frustrated magnetic interactions, which have been discussed in the context of Kitaev's celebrated honeycomb model [9]. The ground state of this model is a gapless $\mathbb{Z}_2$ spin liquid that is stabilized by bond-dependent coupling described by $\mathcal{H} = K_1 \sum_{\langle ij \rangle} S_i^\gamma S_j^\gamma$. Here $\gamma = \{x, y, z\}$ for the three bonds emerging from each lattice site (Fig. 1b). It has been proposed that such interactions with $K_1 < 0$ can arise [10–13] from a delicate balance of spin-orbit coupling (SOC), Hund's coupling, and crystal-field splitting (CFS) that may be approximated in α-$RuCl_3$ [14, 15]. As a result, recent experiments [16–19] have been discussed in the language of static fluxes and Majorana spinons, which represent the exact excitations of the Kitaev spin liquid (KSL) [9, 20, 21]. In practice, however, the zero field ground state of α-$RuCl_3$ exhibits zigzag antiferromagnetic order [22, 23] (Fig. 1a), suggesting deviations from the interactions of the pure Kitaev model. The specific nature of these deviations has been heavily discussed [15, 24–27], with most recent works agreeing additional large anisotropic couplings and long-range exchange likely stabilize magnetic order [25, 26, 28–30]. Understanding the role of these interactions in the dynamic response remains a key challenge.

Dynamical probes, such as inelastic neutron scattering [16–18, 31] (INS) and electron spin resonance [32–34] (ESR), have observed an unconventional continuum of magnetic excitations that coexist with magnons below $T_N \sim 7$ K. The identity of the continuum has captured significant focus, as the connection to the Kitaev model remains an open question. Such continua may arise generically in the presence of bond-dependent anisotropic couplings [28]. Recent interest has therefore

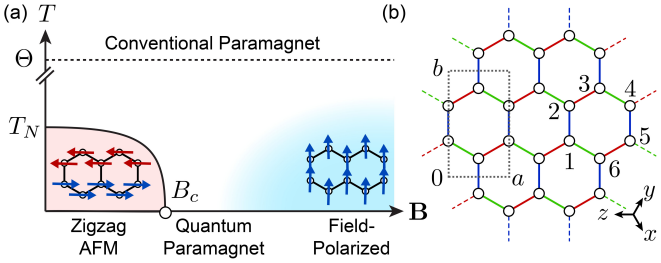

FIG. 1. (a) Schematic phase diagram of the model Hamiltonian (1) for α-$RuCl_3$ at finite T and B. T_N is the Néel temperature, and Θ is the Curie-Weiss constant. The variable blue color shading indicates a crossover to the high-field regime. (b) 24-site cluster employed in ED calculations showing the orientation of the cubic x, y, z axes, and $C2/m$ unit cell. The crystallographic axes correspond to $a = [11\bar{2}]$, $b = [1\bar{1}0]$, and $c^* = [111]$ in cubic coordinates. The numbers label sites defining the $\mathbb{Z}_2$ flux operator $\hat{W}_p$. Nearest neighbour X-,Y-, and Z-bonds are red, green, and blue, respectively.

turned toward regimes where the suppression of zigzag order may reveal the underlying character of the continuum (Fig. 1a). For example, order is suppressed by a small in-plane field of $B_c \sim 7$ T, giving rise to a much-discussed quantum paramagnetic state [35–41]. Such behaviour may be analogous to the response of the 3D iridates β, γ-Li_2IrO_3 [42, 43]. Finally, significant spin correlations persist in α-$RuCl_3$ well above $T_N \sim 7$ K, suggesting a possible unconventional paramagnetic phase at intermediate temperatures [18, 44]. In this work, we discuss the physics in these regimes for a realistic model Hamiltonian for α-$RuCl_3$ proposed in [28] and compare with the available experimental observations.

Model – We focus on a simplified C_3-symmetric four-parameter model that has been shown to reproduce many aspects of the inelastic neutron scattering in the ordered

phase at low temperature and zero field [28]. Specifically:

$$\mathcal{H} = \sum_{\langle ij \rangle} J_1\ \mathbf{S}_i \cdot \mathbf{S}_j + K_1 S_i^\gamma S_j^\gamma + \Gamma_1 \left(S_i^\alpha S_j^\beta + S_i^\beta S_j^\alpha \right) + \sum_{\langle\langle\langle ij \rangle\rangle\rangle} J_3\ \mathbf{S}_i \cdot \mathbf{S}_j - \mu_B \sum_i \mathbf{B} \cdot \mathbf{g} \cdot \mathbf{S}_i \quad (1)$$

with nearest neighbour interactions $J_1 = -0.5$, $K_1 = -5.0$, and $\Gamma_1 = +2.5$ meV and third neighbour interaction $J_3 = +0.5$ meV. The pure Kitaev model corresponds to $J_1 = \Gamma_1 = J_3 = 0$. Here, $\mathbf{g}$ is the anisotropic g-tensor. In the calculations we used $g_{c^*} = 1.3$ and $g_{ab} = 2.3$; these values are consistent with the range of previous theoretical estimates for α-$RuCl_3$ [25, 45], and experimental values for similar compounds [46–48]. We note that this simplified model underestimates the zero-field gap for excitations [16, 31, 32], which may be related to a weak breaking of C_3 symmetry in actual samples [23], or small additional interactions [25, 26].

Results – We first discuss the static correlations at zero temperature, computed via exact diagonalization (ED) on the 24-site cluster in Fig. 1b for $\mathbf{B}||b$. Results for $\mathbf{B}||a$ are similar and are shown in the Supplemental Material [49]. The anisotropy in the computed magnetization (Fig. 2a) agrees well with experimental data at $T = 2$ K, thus providing a consistency check for the present model. At low fields, the static structure factor $\langle \mathbf{S}_{-\mathbf{k}} \cdot \mathbf{S}_{\mathbf{k}} \rangle$ is peaked at the M-, M′-, and Y-points, corresponding to the three possible domains of zigzag order (Fig. 2b). Application of small fields differentiates the zigzag domains, stabilizing $\mathbf{Q} = \mathrm{Y}$ for $\mathbf{B}||b$ and $\mathbf{Q} = \mathrm{M,M'}$ for $\mathbf{B}||a$. For fields $B > B_c \sim 6$ T, the suppression of $\langle \mathbf{S}_{-\mathbf{k}} \cdot \mathbf{S}_{\mathbf{k}} \rangle$ at the zigzag wavevectors, and growth of correlations at $\mathbf{k} = 0$ for both $\mathbf{B}||a, b$, indicates a transition towards a paramagnetic state with a substantial ferromagnetic polarization.

In principle, this transition may occur directly, or proceed via one or more intermediate states [25, 53, 54]. For the present model, we resolve only one phase transition at $B_c \sim 6$ T for both $\mathbf{B}||a, b$, as evidenced by a single peak in the second derivative of the ground state energy ($-\partial^2 E_0/\partial B^2$) and ground state fidelity susceptibility ($\chi_F = \frac{2}{(\delta B)^2}(1 - \langle \Psi_0(B) | \Psi_0(B + \delta B) \rangle)$), shown in Fig. 2c. The appearance of only one transition indicates that the high-field state is adiabatically connected to the fully polarized state and is therefore topologically trivial. The finite value of χ_F at all fields is consistent with a continuous transition, suggesting that T_N may terminate in a quantum critical point at B_c [38] for both $\mathbf{B}||a, b$. This is in contrast to the results of a mean-field analysis, which found the transition with $\mathbf{B}||b$ to be continuous, while for $\mathbf{B}||a$ to be first order [53]. The magnitude of the critical field $B_c \sim 6$ T in ED calculations agrees well with the range of 6 - 8 T observed experimentally [35–40]. The reduction with respect to the classical transition fields of 11 T ($\mathbf{B}||b$) and 8.2 T ($\mathbf{B}||a$) is likely the effect of

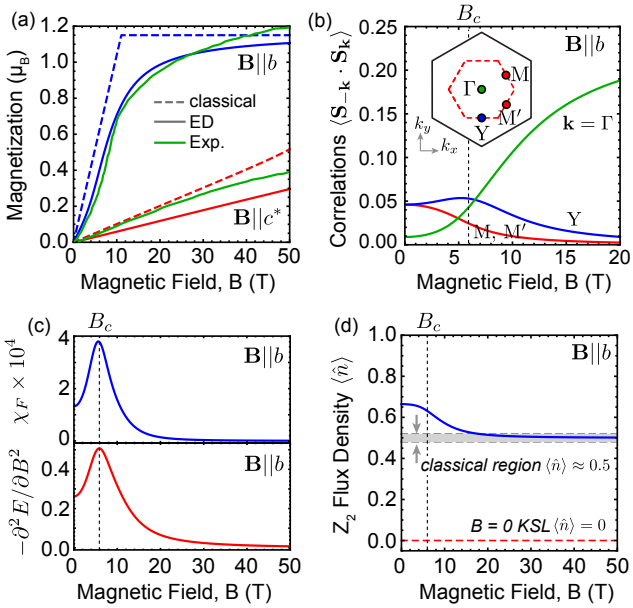

FIG. 2. Evolution of the $T = 0$ static correlations under magnetic field computed via ED. (a) Magnetization $M(B)$. Experimental data at $T = 2$ K from [23]. (b) Static structure factor for $\mathbf{k} = \Gamma$, M, and Y. (c) Ground state fidelity susceptibility χ_F and second derivative of the ground state energy. The peak in both indicates a single phase transition at $B_c \sim 6$ T. (d) $\mathbb{Z}_2$ flux density compared to known limits: the Kitaev spin liquid (KSL) has $\langle \hat{n} \rangle = 0$ at $B = 0$, while classical collinear ordered states have $\langle \hat{n} \rangle \approx 0.5$. The present model has $\langle \hat{n} \rangle \gtrsim 0.5$ at all fields (blue line).

quantum fluctuations. Similarly, the computed magnetization in ED lies below the classical value (Fig. 2a) at all finite fields. In contrast with pure SU(2) Heisenberg interactions, the fully polarized state would not be an eigenstate of $\mathcal{H}$, so that quantum fluctuations reduce the magnetization ($M(B)$) even at high field [23, 53].

In order to further characterize the high- and low-field states, we show, in Fig. 2d, the evolution of the $\mathbb{Z}_2$ flux density appropriate for the KSL. This is $\langle \hat{n} \rangle = \frac{1}{2}(1 - \langle \hat{W}_p \rangle)$, where $\hat{W}_p = 2^6 S_1^x S_2^y S_3^z S_4^x S_5^y S_6^z$ (refer to Fig. 1b for site labels). In the limit of pure K_1 interactions and $B = T = 0$, the KSL has $\langle \hat{W}_p \rangle = +1$ and $\langle \hat{n} \rangle = 0$, signifying the absence of fluxes [9]. In contrast, any classical collinear ordered state must have $\langle \hat{n} \rangle \approx \frac{1}{2}$, which would imply both a large flux density, and a maximum in the variance of the flux density, $\Delta n = \sqrt{\langle \hat{n}^2 \rangle - \langle \hat{n} \rangle^2} \approx \frac{1}{2}$. That is, any state with a sizeable ordered moment cannot have a well-defined $\hat{n}$, since $[\hat{\mathbf{S}}_i, \hat{W}_p] \neq 0$. Numerically, we find that $\langle \hat{n} \rangle$ indeed reaches $\sim \frac{1}{2}$ at high field. Interestingly, at low-field, the computed flux density is even *larger* than this classical value. For $\Gamma_1 > 0$, the energy is minimized for off-diagonal correlations $\langle S_i^\alpha S_j^\beta \rangle < 0$, which effectively enhance $\langle \hat{n} \rangle$.

Given the large $\langle \hat{n} \rangle$ and Δn in the ground state of the

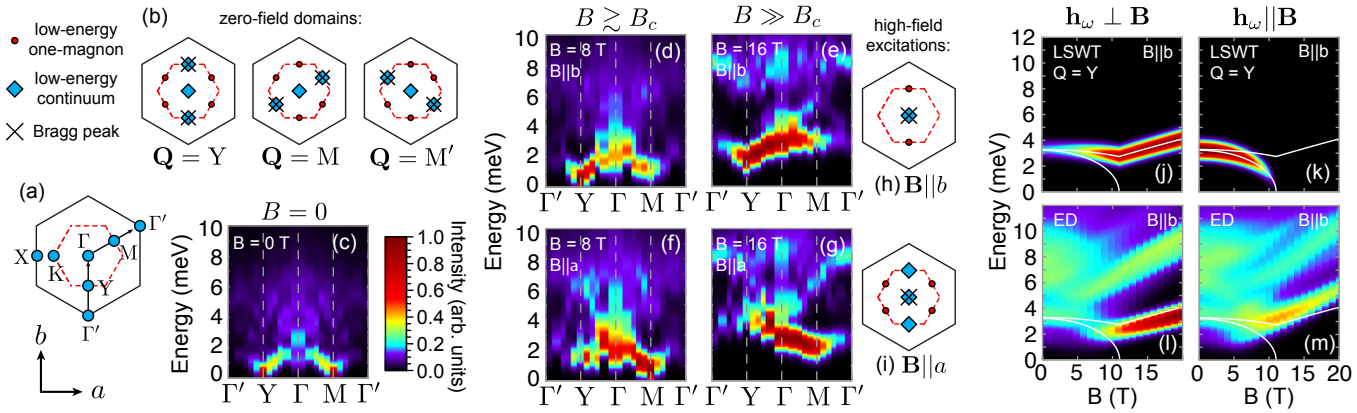

FIG. 3. (a) Brillouin zone definition. (b) Summary of low-energy contributions to $\mathcal{S}^{\mu\nu}$ from different zigzag domains at $B = 0$. (c-g) $T = 0$ inelastic neutron scattering intensity $\mathcal{I}(\mathbf{k},\omega) \propto f(k)^2 \sum_{\mu\nu}(\delta_{\mu,\nu} - \hat{k}_\mu \hat{k}_\nu)\mathcal{S}^{\mu\nu}(\mathbf{k},\omega)$ under applied field, computed with ED; $f(k)$ is the magnetic form factor for Ru^{3+} [55]. (c) $B = 0$, (d,e) $\mathbf{B}||b$, (f,g) $\mathbf{B}||a$. (h,i) Summary of low-energy contributions to $\mathcal{S}^{\mu\nu}$ for $B > B_c$. (j-m) Polarized electron spin resonance absorption $\omega\chi''(\omega) \propto \omega\mathcal{S}^{\mu\mu}(0,\omega)$, with $\mu||\mathbf{h}_\omega$, at the level of (j,k) LSWT and (l,m) ED. LSWT results include only the domain $\mathbf{Q} = \mathrm{Y}$ for $B < B_c$. ED results combine data from various 20- and 24-site clusters as in [28]. Spectra were Gaussian broadened by a width of 0.5 meV, and integrated over k_{c^*} consistent with [17]. The color scale of each figure is independent.

present model at all fields, discussion of the excitations in terms of the fluxes and spinons of the $\mathbb{Z}_2$ KSL may not provide the most appropriate starting point at $T = 0$. Consistently, [54] found all $\mathbb{Z}_2$ states to have poor variational energies for a similar model. We therefore choose the description in terms of magnon and multi-magnon (continuum) excitations, which can be understood perturbatively starting from a mean-field description of the zigzag or field polarized state.

An important consequence of the bond-dependent interactions in real space, is that low-energy contributions to the dynamical structure factor $\mathcal{S}^{\mu\nu}(\mathbf{k},\omega) = \int dt\ e^{-i\omega t}\langle S^\mu_{-\mathbf{k}}(t) S^\nu_{\mathbf{k}}(0)\rangle$ appear at locations in k-space related to the polarization $\mu,\nu \in \{x,y,z\}$ [56]. This observation applies equally to the present model, and to other "Klein-dual" phases [7, 57, 58]. As a result, rotation of the local moments $\mathbf{m}_i(B)$ with respect to the anisotropy axes dramatically restructures the low-energy excitations at finite $\mathbf{B}$, which can be anticipated at the level of LSWT. Here we use the LSWT reference (see Fig. 3b,h,i and the Supplemental Material [49]) to analyze the INS intensity $\mathcal{I}(\mathbf{k},\omega)$ computed via ED calculations.

At zero field the ED response (Fig. 3c) reflects a mixture of the three zigzag domains. We note however that within each domain, the low-energy magnons appear at wavevectors away from the Bragg peak position and a *continuum response is expected near the* Γ*-point*, due to a strong and kinematically allowed decay process for the single magnons [28]. For example, at $B = 0$, the zigzag domain with Bragg peak at Y has low-energy magnons at M and M′, while low-energy (multi-magnon) continuum states appear near the Y- and Γ-points (Fig. 3b). For the latter k-points, the extension of the multi-particle continuum below the single magnon excitations implies the spontaneous decay of magnons, provided coupling to the continuum is symmetry-allowed [59, 60], which is the case for the Hamiltonian in (1). For $\mathbf{B}||b$ and $B > B_c$, the rotation of moments causes the magnons at M and M′ to shift to higher energy, while new soft magnons appear at the Y-point (Fig. 3d,e,h), which is the Bragg peak position of the most stable zigzag domain below B_c. Low-energy continuum excitations remain near the Γ-point, implying the continuum may remain stable at high field. Analogous effects occur for $\mathbf{B}||a$ (Fig. 3f,g,i and Supplemental Material [49]). Specifically for $\mathbf{B}||a$ and $B > B_c$, the lowest-energy magnons appear at M and M′, while the *lowest-energy continuum states* appear at Y and Γ. Together, these results may explain the observed absence of sharp low-energy magnons at high field $\mathbf{B}||a$, along the $\mathbf{k}$-path Γ-Y-Γ' (recently reported in [61]).

The composition of this continuum near $k = 0$ has been a matter of significant discussion, as the breakdown of magnons may signify the emergence of unconventional excitations. To investigate the dynamical response at $k = 0$, we show, in Fig. 3(j-m), the ESR response $\omega\chi''(\omega)$ at the level of ED and LSWT for $\mathbf{B}||b$. Results for $\mathbf{B}||a$ are similar [49]. For $B < B_c$, the ESR response should be dominated by the zigzag domain with Bragg point $\mathbf{Q} = \mathrm{Y}$. At the LSWT level, two intense one-magnon bands are anticipated, labelled $m_1^{||}$ and $m_1^{\perp}$ (Fig. 3j,k), with dominant intensity for oscillating magnetic field $\mathbf{h}_\omega$ polarized $||\mathbf{B}$ and $\perp \mathbf{B}$, respectively. These modes also appear in ED (Fig. 3l,m), with the addition of *broad continuum excitations* centered around 6 - 8 meV, labelled $m_2^{||}$ and $m_2^{\perp}$. The polarization dependence of $\omega\chi''(\omega)$ for $B < B_c$ is likely underestimated in ED due to the per-

sistence of $\mathbf{Q} = \mathrm{M}, \mathrm{M}'$ zigzag correlations resulting from finite-size effects (see Fig. 2b). For fields $B > B_c$, LSWT predicts only one intense one-magnon $\ell_1^{\perp}$ excitation of transverse ($\mathbf{h}_\omega \perp \mathbf{B}$) polarization, while the ED response shows multiple excitation branches. The lowest energy mode $\ell_1^{\perp}$ in ED appears only for $\mathbf{h}_\omega \perp \mathbf{B}$ (Fig. 3l). For this mode, the gap increases linearly with applied field with a rate of $g_{ab}\mu_B\Delta S \approx 0.13$ meV/T, with $\Delta S = 1$, consistent with a one-magnon excitation as predicted by LSWT. A second intense band $\ell_2^{\perp}$ appears at higher energy with larger slope $\Delta S \approx 2$, consistent with a two-magnon excitation. For longitudinal ($\mathbf{h}_\omega || \mathbf{B}$) polarization, the main excitation branches $\ell_1^{||}$ and $\ell_3^{||}$ also evolve with $\Delta S \gtrsim 2$, suggesting a similar multi-magnon origin. Finally, weak higher energy modes $\ell_3^{\perp,||}$ also appear with $\Delta S \geq 2$. These results are in qualitative agreement with recent high-field THz ESR experiments [33], offering a potential interpretation of the observed excitations (for a detailed comparison see the Supplemental Material [49]). In this context, the application of magnetic field is valuable for 'dissecting' the $\mathbf{k} = \Gamma$ continuum. Such an experimental strategy has recently been demonstrated for the pyrochlore $Yb_2Ti_2O_7$ [62, 63], which also features anisotropic bond-dependent interactions.

Having described the effect of magnetic field on the excitations, we now discuss the effects of finite temperature for $B = 0$. Results computed via the Finite Temperature Lanczos method (FTLM) [64] are shown in Fig. 4. Analysis of statistical errors suggests reliable results for $T \gtrsim 5$ K, see [49]. We first estimate $T_N \approx 8$ K from a maximum in $-(\partial/\partial T)\langle \mathbf{S}_{-\mathbf{k}} \cdot \mathbf{S}_{\mathbf{k}} \rangle$, with $\mathbf{k} = \mathrm{M}, \Gamma$. This value is comparable to the experimental values of 7 - 14 K [16, 38, 39]. Upon increasing T above T_N we find a marked shift of the low-energy INS spectral weight away from the zigzag wavevectors, towards the Γ-point (Fig. 4e,f), consistent with INS experiments [16, 61]. Above T_N, the $g_{ab} > g_{c^*}$ emphasizes short-ranged correlations between spin-components in the ab-plane, which are ferromagnetic due to $K_1 < 0$ and $\Gamma_1 > 0$. This is revealed by the positive in-plane Curie-Weiss constant, $\Theta_{ab} \sim -(3J_1 + K_1 - \Gamma_1 + 3J_3)/(4k_B)$, which is $\Theta_{ab} \sim +22$ K for the present model (experimentally, $\Theta_{ab} \sim +38$ to $+68$ K [17, 22, 65]). For this reason, the suppression of zigzag order for $T > T_N$ is expected to generate dominant scattering intensity at $k = 0$, reflecting the emergence of short-ranged ferromagnetic correlations. Overall, the finite temperature spectra agree well with experimental INS observations[18], suggesting that the present model may also capture the essential features of the dynamics above T_N.

An interesting question therefore remains to what extent this region $T_N < T < \Theta$ (Fig. 1a) can be connected to the response of the pure Kitaev model, given the evidence for large Γ_1 interactions in α-$RuCl_3$. For purely Kitaev interactions, the intermediate T regime

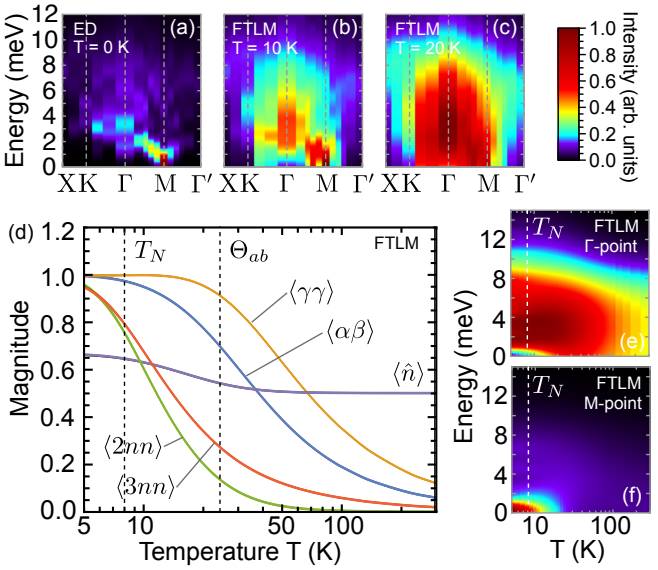

FIG. 4. Neutron scattering intensity for $T > 0$, as a function of $\mathbf{k}$ (a-c) and T for (e) $\mathbf{k} = \Gamma$ and (f) $\mathbf{k} = \mathrm{M}$, combining results of multiple clusters. (d): Kitaev flux density $\langle\hat{n}\rangle$ and normalized real space static correlations computed for the cluster in Fig. 1b, for first nearest neighbours $\langle\gamma\gamma\rangle \equiv \langle S_1^{\gamma} S_2^{\gamma}\rangle_T$, $\langle\alpha\beta\rangle \equiv \langle S_1^{\alpha} S_2^{\beta}\rangle_T$, second neighbours $\langle 2nn\rangle \equiv \langle \mathbf{S}_1 \cdot \mathbf{S}_3\rangle_T$, and third neighbours $\langle 3nn\rangle \equiv \langle \mathbf{S}_1 \cdot \mathbf{S}_4\rangle_T$. Except for $\langle\hat{n}\rangle$, values are normalized by their $T = 0$ value. Site labels refer to Fig. 1b. The color scale of each figure is independent.

would be characterized by a large density of thermally excited fluxes [66, 67], which likely confine the fermionic spinons [7, 44]. This regime is characterized by a saturation of nearest neighbour spin-spin correlations. For the present model, we find deviations from Curie-Weiss behaviour below $T \sim 70$ K, while nearest neighbour correlations saturate for $T \lesssim \Theta_{ab}$ (Fig. 4d). Longer range correlations set in near $T_N \sim 8$ K, suggesting the intermediate temperature regime may be relatively narrow. If the ordering of fluxes at low temperatures is preempted by magnetic order, then a deconfined region may not appear. Consistent with this picture, we find that the Kitaev flux density remains $\langle\hat{n}\rangle \gtrsim \frac{1}{2}$ at all temperatures for the present model (Fig. 4d). This leaves two possibilities for the intermediate temperature dynamics. Either, *all* correlations are short-ranged, suggesting the phase cannot be qualitatively distinguished from a conventional paramagnet, or there exist higher order long-range or algebraic spin correlations. These could be associated with alternative quantum ground states suggested for finite Γ_1 interactions [29, 30, 68], which are not characterized by $\langle\hat{n}\rangle$. In this sense, development of probes for higher order correlations (such as RIXS [69]) may prove vital for further understanding the intermediate T regime. Investigating the $T > 0$ classical dynamics [44] of the full $(J_1, K_1, \Gamma_1, J_3)$ model also represents an important avenue of future study.

Conclusions – We have shown that the model for α-$RuCl_3$ defined in Eq. (1) reproduces many key aspects of the experimental observations, including the relevant energy scales (B_c and T_N), and the evolution of the dynamical response at finite T and $\mathbf{B}$. In the range of T and B studied, we do not find any regime where the $\mathbb{Z}_2$ fluxes of the Kitaev form ($\hat{W}_p$) are dilute, which hampers possible connections to Kitaev's exact solution. We find the high-field phase to be smoothly connected to the fully polarized state. Nonetheless, the evolution of high field excitations reveals significant multiparticle character in the Γ-point continuum, providing insight into recent ESR experiments. Combined, these results supply a valuable framework for interpreting a wide range of recent studies of α-$RuCl_3$.

Acknowledgements – We acknowledge useful discussions with A. Banerjee, C. Batista, A. L. Chernyshev, Y. B. Kim, D. Kovrizhin, J. Knolle, A. Loidl, R. Moessner, and S. E. Nagler. S. M. W. acknowledges support through an NSERC Canada Postdoctoral Fellowship. R. V. and K. R. acknowledge support by the Deutsche Forschungsgemeinschaft through grant SFB/TR 49 and the computer time was allotted by the centre for supercomputing (CSC) in Frankfurt. R. C. was supported in part by KITP under Grant No. NSF PHY-1125915.

[1] L. Savary and L. Balents, Rep. Prog. Phys. **80**, 016502 (2017).
[2] M. R. Norman, Rev. Mod. Phys. **88**, 041002 (2016).
[3] Y. Zhou, K. Kanoda, and T.-K. Ng, Rev. Mod. Phys. **89**, 025003 (2017).
[4] S. Trebst, arXiv preprint arXiv:1701.07056 (2017).
[5] R. Schaffer, E. K.-H. Lee, B.-J. Yang, and Y. B. Kim, Rep. Prog. Phys. **79**, 094504 (2016).
[6] J. G. Rau, E. K.-H. Lee, and H.-Y. Kee, Annu. Rev. Condens. Matter Phys. **7**, 195 (2016).
[7] M. Hermanns, I. Kimchi, and J. Knolle, arXiv preprint arXiv:1705.01740 (2017).
[8] S. M. Winter, A. A. Tsirlin, M. Daghofer, J. van den Brink, Y. Singh, P. Gegenwart, and R. Valentí, J. Phys. Condens. Matter **29**, 493002 (2017).
[9] A. Kitaev, Ann. Phys. **321**, 2 (2006).
[10] G. Jackeli and G. Khaliullin, Phys. Rev. Lett. **102**, 017205 (2009).
[11] J. Chaloupka, G. Jackeli, and G. Khaliullin, Phys. Rev. Lett. **110**, 097204 (2013).
[12] J. G. Rau, E. K.-H. Lee, and H.-Y. Kee, Phys. Rev. Lett. **112**, 077204 (2014).
[13] J. G. Rau and H.-Y. Kee, arXiv preprint arXiv:1408.4811 (2014).
[14] K. W. Plumb, J. P. Clancy, L. J. Sandilands, V. V. Shankar, Y. F. Hu, K. S. Burch, H.-Y. Kee, and Y.-J. Kim, Phys. Rev. B **90**, 041112 (2014).
[15] H.-S. Kim, V. V. Shankar, A. Catuneanu, and H.-Y. Kee, Phys. Rev. B **91**, 241110 (2015).
[16] A. Banerjee, C. A. Bridges, J.-Q. Yan, A. A. Aczel, L. Li, M. B. Stone, G. E. Granroth, M. D. Lumsden, Y. Yiu, J. Knolle, S. Bhattacharjee, D. L. Kovrizhin, R. Moessner, D. A. Tennant, G. Mandrus, and S. E. Nagler, Nat. Mater. **15**, 733 (2016).
[17] A. Banerjee, J. Yan, J. Knolle, C. A. Bridges, M. B. Stone, M. D. Lumsden, D. G. Mandrus, D. A. Tennant, R. Moessner, and S. E. Nagler, Science **356**, 1055 (2017).
[18] S.-H. Do, S.-Y. Park, J. Yoshitake, J. Nasu, Y. Motome, Y. S. Kwon, D. T. Adroja, D. J. Voneshen, K. Kim, T.-H. Jang, J.-H. Park, K.-Y. Choi, and S. Ji, arXiv preprint arXiv:1703.01081 (2017).
[19] J. Nasu, J. Knolle, D. L. Kovrizhin, Y. Motome, and R. Moessner, Nat. Phys. **12**, 912 (2016).
[20] J. Knolle, D. L. Kovrizhin, J. T. Chalker, and R. Moessner, Phys. Rev. B **92**, 115127 (2015).
[21] J. Knolle, D. L. Kovrizhin, J. T. Chalker, and R. Moessner, Phys. Rev. Lett. **112**, 207203 (2014).
[22] J. A. Sears, M. Songvilay, K. W. Plumb, J. P. Clancy, Y. Qiu, Y. Zhao, D. Parshall, and Y.-J. Kim, Phys. Rev. B **91**, 144420 (2015).
[23] R. D. Johnson, S. C. Williams, A. A. Haghighirad, J. Singleton, V. Zapf, P. Manuel, I. I. Mazin, Y. Li, H. O. Jeschke, R. Valentí, and R. Coldea, Phys. Rev. B **92**, 235119 (2015).
[24] H.-S. Kim and H.-Y. Kee, Phys. Rev. B **93**, 155143 (2016).
[25] R. Yadav, N. A. Bogdanov, V. M. Katukuri, S. Nishimoto, J. van den Brink, and L. Hozoi, Sci. Rep. **6**, 37925 (2016).
[26] S. M. Winter, Y. Li, H. O. Jeschke, and R. Valentí, Phys. Rev. B **93**, 214431 (2016).
[27] Y. S. Hou, H. J. Xiang, and X. G. Gong, Phys. Rev. B **96**, 054410 (2017).
[28] S. M. Winter, K. Riedl, P. A. Maksimov, A. L. Chernyshev, A. Honecker, and R. Valentí, Nat. Commun. **8**, 1152 (2017).
[29] M. Gohlke, G. Wachtel, Y. Yamaji, F. Pollmann, and Y. B. Kim, arXiv preprint arXiv:1706.09908 (2017).
[30] A. Catuneanu, Y. Yamaji, G. Wachtel, H.-Y. Kee, and Y. B. Kim, arXiv preprint arXiv:1701.07837 (2017).
[31] K. Ran, J. Wang, W. Wang, Z.-Y. Dong, X. Ren, S. Bao, S. Li, Z. Ma, Y. Gan, Y. Zhang, J. T. Park, G. Deng, S. Danilkin, S.-L. Yu, J.-X. Li, and J. Wen, Phys. Rev. Lett. **118**, 107203 (2017).
[32] A. Little, L. Wu, P. Lampen-Kelley, A. Banerjee, S. Patankar, D. Rees, C. A. Bridges, J.-Q. Yan, D. Mandrus, S. E. Nagler, and J. Orenstein, Phys. Rev. Lett. **119**, 227201 (2017).
[33] Z. Wang, S. Reschke, D. Hüvonen, S.-H. Do, K.-Y. Choi, M. Gensch, U. Nagel, T. Rõõm, and A. Loidl, Phys. Rev. Lett. **119**, 227202 (2017).
[34] A. N. Ponomaryov, E. Schulze, J. Wosnitza, P. Lampen-Kelley, A. Banerjee, J.-Q. Yan, C. A. Bridges, D. G. Mandrus, S. E. Nagler, A. K. Kolezhuk, and S. A. Zvyagin, Phys. Rev. B **96**, 241107 (2017).
[35] S.-H. Baek, S.-H. Do, K.-Y. Choi, Y. S. Kwon, A. U. B. Wolter, S. Nishimoto, J. van den Brink, and B. Büchner, Phys. Rev. Lett. **119**, 037201 (2017).
[36] J. Zheng, K. Ran, T. Li, J. Wang, P. Wang, B. Liu, Z.-X. Liu, B. Normand, J. Wen, and W. Yu, Phys. Rev. Lett. **119**, 227208 (2017).
[37] R. Hentrich, A. U. B. Wolter, X. Zotos, W. Brenig, D. Nowak, A. Isaeva, T. Doert, A. Banerjee, P. Lampen-Kelley, D. G. Mandrus, S. E. Nagler, J. Sears, Y.-J. Kim, B. Büchner, and C. Hess, arXiv preprint

arXiv:1703.08623 (2017).
[38] A. U. B. Wolter, L. T. Corredor, L. Janssen, K. Nenkov, S. Schönecker, S.-H. Do, K.-Y. Choi, R. Albrecht, J. Hunger, T. Doert, M. Vojta, and B. Büchner, Phys. Rev. B **96**, 041405 (2017).
[39] J. A. Sears, Y. Zhao, Z. Xu, J. W. Lynn, and Y.-J. Kim, Phys. Rev. B **95**, 180411 (2017).
[40] I. A. Leahy, C. A. Pocs, P. E. Siegfried, D. Graf, S.-H. Do, K.-Y. Choi, B. Normand, and M. Lee, Phys. Rev. Lett. **118**, 187203 (2017).
[41] Z. Zhu, I. Kimchi, D. N. Sheng, and L. Fu, arXiv preprint arXiv:1710.07595 (2017).
[42] A. Ruiz, A. Frano, N. P. Breznay, I. Kimchi, T. Helm, I. Oswald, J. Y. Chan, R. J. Birgeneau, Z. Islam, and J. G. Analytis, arXiv preprint arXiv:1703.02531 (2017).
[43] K. A. Modic, B. J. Ramshaw, J. B. Betts, N. P. Breznay, J. G. Analytis, R. D. McDonald, and A. Shekhter, Nat. Commun. **8**, 180 (2017).
[44] A. M. Samarakoon, A. Banerjee, S.-S. Zhang, Y. Kamiya, S. E. Nagler, D. A. Tennant, S.-H. Lee, and C. D. Batista, Phys. Rev. B **96**, 134408 (2017).
[45] J. Chaloupka and G. Khaliullin, Phys. Rev. B **94**, 064435 (2016).
[46] J. A. Stanko, H. J. Peresie, R. A. Bernheim, R. Wang, and P. S. Wang, Inorg. Chem. **12**, 634 (1973).
[47] H. S. Jarrett, J. Chem. Phys. **27**, 1298 (1957).
[48] K. S. Pedersen, J. Bendix, A. Tressaud, E. Durand, H. Weihe, Z. Salman, T. J. Morsing, D. N. Woodruff, Y. Lan, W. Wernsdorfer, C. Mathonière, S. Piligkos, S. I. Klokishner, S. Ostrovsky, K. Ollefs, F. Wilhelm, A. Rogalev, and R. Clérac, Nat. Commun. **7**, 12195 (2016).
[49] See Supplemental Material at XX for the discussion of ED results for $\mathbf{B}||a$, a more detailed comparison of ED with ESR experiments, the analysis of low-energy excitations at finite field in LSWT, and further details of the ED and FTLM calculations, which includes Refs. [50–52].
[50] S. K. Choi, R. Coldea, A. N. Kolmogorov, T. Lancaster, I. I. Mazin, S. J. Blundell, P. G. Radaelli, Y. Singh, P. Gegenwart, K. R. Choi, S.-W. Cheong, P. J. Baker, C. Stock, and J. Taylor, Phys. Rev. Lett. **108**, 127204 (2012).
[51] E. Dagotto, Reviews of Modern Physics **66**, 763 (1994).
[52] A. C. Davison and D. V. Hinkley, *Bootstrap methods and their application* (Cambridge University Press, 1997).
[53] L. Janssen, E. C. Andrade, and M. Vojta, Phys. Rev. B **96**, 064430 (2017).
[54] Z.-X. Liu and B. Normand, arXiv preprint arXiv:1709.07990 (2017).
[55] D. T. Cromer and J. T. Waber, Acta Cryst. **18**, 104 (1965).
[56] J. Chaloupka and G. Khaliullin, Phys. Rev. B **92**, 024413 (2015).
[57] I. Kimchi and R. Coldea, Phys. Rev. B **94**, 201110 (2016).
[58] I. Kimchi and A. Vishwanath, Phys. Rev. B **89**, 014414 (2014).
[59] M. E. Zhitomirsky and A. L. Chernyshev, Rev. Mod. Phys. **85**, 219 (2013).
[60] P. A. Maksimov and A. L. Chernyshev, Phys. Rev. B **93**, 014418 (2016).
[61] A. Banerjee, P. Lampen-Kelley, J. Knolle, C. Balz, A. A. Aczel, B. Winn, Y. Liu, D. Pajerowski, J.-Q. Yan, C. A. Bridges, A. T. Savici, B. C. Chakoumakos, M. D. Lumsden, D. A. Tennant, R. Moessner, D. G. Mandrus, and S. E. Nagler, arXiv preprint arXiv:1706.07003 (2017).
[62] J. D. Thompson, P. A. McClarty, D. Prabhakaran, I. Cabrera, T. Guidi, and R. Coldea, Phys. Rev. Lett. **119**, 057203 (2017).
[63] L. Pan, S. K. Kim, A. Ghosh, C. M. Morris, K. A. Ross, E. Kermarrec, B. D. Gaulin, S. M. Koohpayeh, O. Tchernyshyov, and N. P. Armitage, Nat. Commun. **5**, 4970 (2014).
[64] J. Jaklič and P. Prelovšek, Physical Review B **49**, 5065 (1994).
[65] M. Majumder, M. Schmidt, H. Rosner, A. A. Tsirlin, H. Yasuoka, and M. Baenitz, Phys. Rev. B **91**, 180401 (2015).
[66] J. Nasu, M. Udagawa, and Y. Motome, Phys. Rev. B **92**, 115122 (2015).
[67] J. Yoshitake, J. Nasu, Y. Kato, and Y. Motome, Phys. Rev. B **96**, 024438 (2017).
[68] I. Rousochatzakis and N. B. Perkins, Phys. Rev. Lett. **118**, 147204 (2017).
[69] G. B. Halász, N. B. Perkins, and J. van den Brink, Phys. Rev. Lett. **117**, 127203 (2016).